Epidemic spreading in temporal and adaptive networks with static backbone

Epidemic spreading in temporal and adaptive networks with static backbone

Matthieu Nadini, Alessandro Rizzo, *Senior Member, IEEE,* Maurizio Porfiri, *Fellow, IEEE*

Abstract—Activity-driven networks (ADNs) are a powerful paradigm to study epidemic spreading in temporal networks, where the dynamics of the disease and the evolution of the links share a common time-scale. One of the key assumptions of ADNs is the lack of preferential connections among individuals. This assumption hinders the application of ADNs to several realistic scenarios where some contacts persist in time, rather than intermittently activate. Here, we examine an improved modeling framework that superimposes an ADN to a static backbone network, toward the integration of persistent contacts with time-varying connections. To demonstrate the interplay between the ADN and the static backbone, we investigate the effect of behavioral changes on the disease dynamics. In this framework, each individual may adapt his/her activity as a function of the health status, thereby adjusting the relative weight of time-varying versus static links. To illustrate the approach, we consider two classes of backbone networks, Erdős-Rényi and random regular, and two disease models, SIS and SIR. A general mean-field theory is established for predicting the epidemic threshold, and numerical simulations are conducted to shed light on the role of network parameters on the epidemic spreading and estimate the epidemic size.

Index Terms—Activity-driven, behavior, epidemic threshold, mean-field, time-varying network

1 Introduction

Temporal networks have been recently gaining momentum for their tremendous potential to accurately model complex dynamical systems [1], [2]. Temporal networks can encapsulate fundamental characteristics of complex systems, including the intricate interplay between node and connection dynamics. Among the possible fields of applications of temporal networks, epidemiology has been one of the most studied, with pioneering efforts appearing in the late 1980s and 1990s [3], [4], [5]. Research on the application of temporal networks in epidemiology is extremely active and steadily fueled by new time-resolved datasets, theories, concepts, algorithms, and measurements [6].

Contacts between individuals that support the transmission of infections are dynamical in nature. The evolution of these contacts, in turn, is determined by human behavior, introducing an internal dependence between nodes' and links' dynamics [7]. Activity-driven networks (ADNs) promise a tractable study of the co-evolution, at comparable time-scales, of the link formation and individual node dynamics. The ADN paradigm overcomes the limitations imposed by time-scale separation, which would otherwise yield annealed or aggregated representations of the network evolution [8]. Classical infection and diffusion processes have been modeled through ADNs calibrated on synthetic population models [9], [10]. In this context, different aspects have been investigated, including characteristics of the epidemic threshold [11], [12], along with the percolation time and its relationship with epidemic spreading [13]. From a theoretical point of view, an equivalent continuous-time discrete-activity ADN model has been recently established to gain new analytical insight, improve predictions, and mitigate the confounds related to the selection of the sampling time in discrete-time schemes [14], [15].

In its original incarnation, an ADN draws the connections between nodes at random, without any prior knowledge of social or geographic relationships that may favor one link over another. In other words, at any time, a node may connect with any other nodes in the network. However, when modeling real networks, this assumption severely challenges the feasibility of the ADN paradigm. For example, networks of contacts in epidemic spreading are characterized by memory effects and non-Markovian patterns [16], as well as community structures [17]. Considerable effort has been devoted to introducing features in ADN-based modeling of epidemic phenomena, toward a faithful representation and prediction of realistic epidemic processes. Significant milestones have been reached through the introduction of memory effects in the link formation [18], presence of communities [19], and co-existence of a static network backbone and an ADN [20]. The introduction of the effect of individual behavior due to the health status or awareness of the spreading [7] has fostered an ADN-based model of Ebola spreading in the 2014 Liberia outbreak [21].

While individuals may intermittently come in contact arbitrarily or by choice, some links tend to be persistent in time, such as those generated in the household, at work, and with close friends. These links are identified by sociologists

- *M. Nadini is with the Department of Mechanical and Aerospace Engineering, New York University Tandon School of Engineering, Brooklyn, New York 11201, USA. E-mail: mn2415@nyu.edu.*
- *A. Rizzo is with the Office of Innovation, New York University Tandon School of Engineering, Brooklyn, New York 11201, USA, and with Dipartimento di Elettronica e Telecomunicazioni, Politecnico di Torino, 10129 Torino, ITALY. E-mail: alessandro.rizzo@polito.it.*
- *M. Porfiri is with the Department of Mechanical and Aerospace Engineering and also with the Department of Biomedical Engineering, New York University Tandon School of Engineering, Brooklyn, NY 11201. E-mail: mporfiri@nyu.edu.*

(Corresponding authors: Alessandro Rizzo and Maurizio Porfiri.)

as the structure of "strong ties", as opposed to "weak ties" that correspond to intermittent connections from causal encounters or acquaintances [22], [23]. Such heterogeneity plays a fundamental role in spreading processes over social networks, often yielding counter-intuitive phenomena. For example, in [24], the analysis of a large database of mobile communications reveals that the network is robust to the removal of strong ties but tends to collapse after a phase transition when weak ties are removed. In [25], the analysis of the classic rumor spreading model over both synthetic and real networks suggests that strong ties inhibit information diffusion by confining communication within groups of strongly connected users. In [26], the presence of weak ties in a communication network is shown to dramatically increase the length of the observation interval that is required for estimating time-averaged network properties. The important role of weak ties on the outcome of epidemic spreading is further echoed by [27]. Models and methods to incorporate heterogeneity in the strength of the ties and quantify its effect are key to a correct prediction of the spreading outcome, such as the computation of the epidemic threshold, prevalence, and incidence.

While it is difficult to precisely quantify the strength of a tie and isolate static from time-varying links [28], recent efforts have attempted to establish a rigorous mathematical basis for the study of ADNs with coexisting time-varying and static links [20], [29], [30]. In [29], a non-Markovian memory phenomenon is introduced to model time recurrence of the links. In [30], a community structure is constructed to model strong ties via intra-community connections and weak ties via inter-community links. In [20], the combination of a static backbone, associated with strong ties, and an ADN, comprising weak ties, is considered. The terminology used by the authors to identify this combined network is *static and activity-driven coupling network.* Toward the design of realistic models, the static and the time-varying networks of contacts can be inferred and designed independently, even from different data sources. For example, in studying the spreading of influenza in a community, the static backbone might be inferred from the city registries and by interviews in social circles, whereas intermittent contacts might be estimated by positioning sensors or statistical inferences on mobility models. Despite its practical and theoretical promises, several advancements to [20] should be undertaken before its application to real-world problems.

Here, we seek to extend the work in [20] along two main research directions. First, we include an adaptive mechanism that accounts for the effect of changes in individual behavior associated with their health status. Modeling individual behavior in the spreading of epidemic diseases has been shown to be crucial in many epidemiological applications [31], [32], [33], [34], [35]. For example, infections of respiratory tracts, such as influenza, MERS-CoV, or SARS, are known to hamper the activity of individuals [36], [37], [38], [39], thereby challenging the application of standard ADN approaches where the activity of individuals is constant in time. Second, we model strong ties by accounting for more realistic topologies than in [20]. In [20], the strong structure is modeled through an Erdős-Rényi (ER) [40] network, whose value is limited when predicting epidemic spreading in real-world applications [41].

Starting from the definition of the novel modeling framework, this paper unfolds along several directions, using as epidemic benchmarks the well-known Susceptible-Infected-Susceptible (SIS) and Susceptible-Infected-Recovered (SIR) processes [42]. Two different network types are adopted to model static backbones, that is, ER and random regular (RR) networks. The former is used to offer a term of comparison with [20] and assess how behavioral changes affect the spreading of the disease. The latter is introduced to present a more realistic representation of the static backbone, toward modeling epidemics in large-size networks [43], [44], [45]. First, we analytically study salient topological features of the network of contacts, investigating the effects of the epidemic spreading on the degree distribution through the adaptive mechanism. Then, we characterize the epidemic model by determining its epidemic threshold and quantifying the role of the static backbone on the network resilience (defined as the propensity of the network to the inception of the epidemic spreading). Finally, extensive simulations are conducted, aiming at unraveling the intricate interplay among topological, behavioral, and epidemic features on the outcome of the epidemic spreading.

The paper is organized as follows. In Section 2, we introduce the proposed model and summarize the studied epidemic processes. In Section 3, we present an analytical study of the model, focusing on the degree distribution and the average degree of the integrated network of contacts. In Section 4, we analytically determine the epidemic thresholds for both the SIS and SIR models. In Section 5, we report an extensive simulation campaign to validate our analytical findings and quantify the epidemic size. In Section 6, we summarize our results and draw our main conclusions.

2 Modeling framework

We consider a network of N nodes, labeled with $i = 1, \ldots, N$. At a given discrete time instant $t \in \mathbb{N}$, each node takes only one of the possible states in the discrete set $\mathcal{X} \triangleq \{x_1, \ldots, x_M\}$, where M is the number of states. Each state is associated with a particular epidemiological condition. For example, in an SIS epidemic model, nodes can be either Susceptible (S) or Infected (I), such that $\mathcal{X} = \{S, I\}$; while, in an SIR epidemic model, nodes can also become Recovered/Removed (R), such that $\mathcal{X} = \{S, I, R\}$ [46].

We examine two different types of links between nodes: static and time-varying. Static links correspond to interactions between family members and close friends [47], which are expected to evolve at a much slower rate than the dynamics of the disease. These links constitute the backbone of the network [26], therefore their topology should be assimilated to a homogeneous network of small maximum degree [48]. Here, we consider two potential instances for the backbone network. First, we examine an ER network [40], with Poissonian degree distribution $P(k_{\mathrm{st}})$, similar to [20]. Then, we study an RR network [49], whose epidemic threshold is expected to offer an improved estimate for large random backbones [43], [44], [45].

The evolution of time-varying links is modeled using the ADN paradigm [7], [8], [50], [51]. In this network, each node i has an activity rate a_{i,x_j}, which represents the probability in a unit time that node i in state x_j generates dynamic

links with any other node in the network. The activity rate is constructed upon two parameters: the activity potential α_i of node i and the behavioral coefficient η_{x_j} of state x_j. The activity potential α_i is a constant quantity obtained as the realization of a random variable with distribution $F(\alpha)$. The behavioral coefficient η_{x_j} is a state-dependent scaling factor of the activity potential, which takes non-negative values as a function of the mode of epidemic spreading. For example, $\eta_{x_j} \in \{\eta_S, \eta_I\}$ for SIS models and $\eta_{x_j} \in \{\eta_S, \eta_I, \eta_R\}$ for SIR models. The activity rate is ultimately computed as $a_{i,x_j} = \eta_{x_j}\alpha_i$.

Based upon previous studies [7], [21], [52], we posit that the distribution of the activity potentials follows a power law with cut-offs, that is, $F(\alpha) \propto \alpha^{-\gamma}$, with $\alpha \in [\alpha_{\min}, \alpha_{\max}]$. To define the activity potential as a probability in a unit time and avoid divergence of the distribution close to zero, we set the higher cut-off to $\alpha_{\max} = (\eta_{\max}\Delta t)^{-1}$, where $\eta_{\max}$ is the largest value of the behavioral coefficient in the epidemic model and Δt is the time increment[1], and the lower cut-off [2] to $\alpha_{\min} = \epsilon/\eta_{\max}$, where ϵ is a small parameter, here chosen to be $\epsilon = 10^{-3}$. Grounded in experimental observations from the technical literature [21], [52], the exponent of the power law distribution of the activity potentials should be in the interval $2 \leq \gamma \leq 3$.

The network of contacts is the superposition of two graphs, the static graph, $G_{\rm st}$, representative of the backbone, and the ADN, $G^t_{\rm ADN}$, modeling the evolution of the time-varying links.

Neither of the graphs, $G_{\rm st}$ and $G^t_{\rm ADN}$, has self-loops and multiedges, but multiedges might be observed in the network of contacts, G^t. These multiedges correspond to the time-varying links that are activated by the ADN where a static link already exists. In the thermodynamic limit ($N \to +\infty$), networks with backbones of bounded degree distribution, the probability that a multiedge is formed is negligible. In this case, the network of contacts can be assimilated to a standard graph, corresponding to the superposition of $G_{\rm st}$ and $G^t_{\rm ADN}$ [53].

The generative process of the network of contacts G^t is similar to the process presented in [20], with the exception of the activity, which is treated as a state-dependent quantity in our formulation. It is created through the following rules:

(i) at $t = 0$, a static network $G_{\rm st}$ with a degree distribution $P(k_{\rm st})$ is generated;
(ii) at every discrete time step t, each node i in the network becomes active with probability $a_{i,x_j}\Delta t$, and creates m links with random nodes selected from a uniform distribution;
(iii) the epidemic dynamics takes place over the network G^t; and
(iv) at the next time step $t + \Delta t$, all the links in $G^t_{\rm ADN}$ are deleted and the process resumes from step (ii).

An illustration of the generative process is given in Fig. 1.

1. The upper cut-off is required for ensuring that the probability of creating a link is less than one, although this might also be enforced in an approximate manner by properly selecting the time scale of the network assembly.

2. The value of the lower cut-off can be changed without loss of generality.

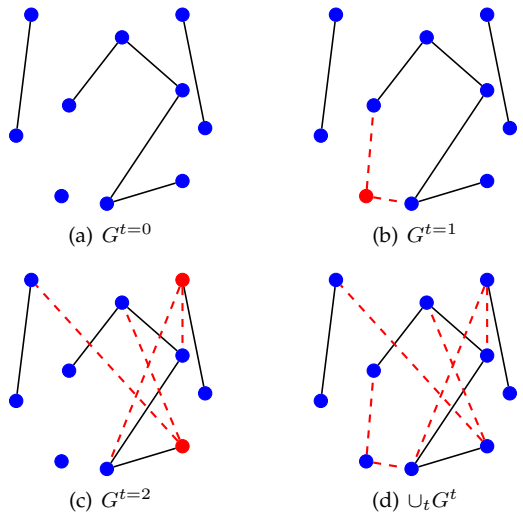

Fig. 1. Schematic representation of the generative process of the network of contacts with $\Delta t = 1$. Panel (a): at time $t = 0$, the static backbone is generated. Panels (b-c): two independent time-varying structures are constructed and superimposed to the static network. Active nodes are displayed in red and create respectively $m = 2$ links to randomly selected nodes. Panel (d): time-integrated network comprising all the links generated in the observation time.

3 Analytical Insight on the Average Degree and Degree Distribution

Here, we examine salient topological features of the network of contacts in the thermodynamic limit. First, we discuss how the expected average degree is affected by the disease spreading in the network. We demonstrate a relationship between the epidemic threshold and the expected average degree, which helps clarifying the role of behavioral changes on epidemic spreading. Second, we examine in detail the degree distribution, illustrating the onset of a heavy-tail distribution, similar to many real systems [54], [55], [56].

We specialize our treatment to SIS and SIR models. The SIS model is fully characterized by two transitions. The first transition describes the infection propagation, such that, a susceptible node in contact with an infected individual becomes infected with probability λ. The second transition encapsulates the recovery process, where infected nodes spontaneously return in the susceptible state with probability μ. Also, the SIR model is fully characterized by two transitions. The infection propagation is equivalent to the SIS process, while the second transition describes how infected individuals recover spontaneously and permanently with probability μ. However, our framework is valid for a more general setup with M discrete states, whose derivation is presented in the Appendix. In the following, we adhere to the following notation: given a network-related quantity $*$, we call $\langle * \rangle$ its statistical average over the network and $\mathrm{E}[*]$ its expected value across multiple independent realizations.

3.1 Average degree

By construction, the expected average degree $\mathrm{E}\left[\langle k^t \rangle\right]$ of the network of contacts is composed of the sum of two average degrees: the constant average degree of the static backbone, $\langle k_{\rm st} \rangle$, and the expected value of the average degree of time-

varying links, $\mathrm{E}\left[\langle k^t_{\mathrm{ADN}}\rangle\right]$. The latter value depends on the number of nodes in each of the states of the epidemic model.

The expected value of the average degree in the SIS model is (details in the Appendix)

$$\begin{aligned}\mathrm{E}\left[\langle k^t\rangle\right] &= \langle k_{\mathrm{st}}\rangle + \mathrm{E}\left[\langle k^t_{\mathrm{ADN}}\rangle\right] \\ &= \langle k_{\mathrm{st}}\rangle + \frac{2m}{N}\left(\eta_S\langle\alpha^t_S\rangle S^t + \eta_I\langle\alpha^t_I\rangle I^t\right),\end{aligned} \tag{1}$$

where $\langle\alpha^t_S\rangle$ and $\langle\alpha^t_I\rangle$ are the average activity potentials over all nodes in the susceptible and infected states at time t, respectively. Further, S^t and I^t are the number of nodes in the susceptible and infected states, respectively. Similarly, in the SIR model, we find (details in the Appendix)

$$\begin{aligned}\mathrm{E}\left[\langle k^t\rangle\right] &= \langle k_{\mathrm{st}}\rangle + \mathrm{E}\left[\langle k^t_{\mathrm{ADN}}\rangle\right] \\ &= \langle k_{\mathrm{st}}\rangle + \frac{2m}{N}\left(\eta_S\langle\alpha^t_S\rangle S^t + \eta_I\langle\alpha^t_I\rangle I^t + \eta_R\langle\alpha^t_R\rangle R^t\right),\end{aligned} \tag{2}$$

where $\langle\alpha^t_R\rangle$ is the average activity potentials in the recovered state at time t, and R^t is the number of nodes in the recovered state.

If behavioral changes are discarded, that is, $\eta_S = \eta_I = \eta_R = \eta$, the average degree of the time-varying links in Eqs. (1) and (2) reads $\mathrm{E}\left[\langle k^t_{\mathrm{ADN}}\rangle\right] = 2m\eta\langle\alpha\rangle$, in agreement with the original computation [8]. When individuals change their behavior according to their health states, that is, $\eta_S \neq \eta_I \neq \eta_R$, Eqs. (1) and (2) are influenced by the temporal trend of the number of susceptible, infected, and recovered nodes. To demonstrate this influence, in Fig. 2, we present a realization of the SIS in the presence of behavioral changes and compare its expected average degree, given in Eq. (1) with the expected average degree for the ADN without behavioral change. In the presence of behavioral changes, we set $\eta_I < \eta_S$ to proxy an activity reduction for infected individuals [36], [37], [38], [39]. From Fig. 2, we observe that an increase in the number of infected nodes reduces the overall propensity to generating links, thereby decreasing the average connectivity in the network.

3.2 Degree distribution

To confirm that our model encapsulates the heterogeneity observed in many real systems [54], [55], [56], we investigate the degree distribution of the network of contacts. By construction, our model comprises two independent degree distributions, one for the static backbone and one for the ADN, respectively. The former, $P(k_{\mathrm{st}})$, is constant in time and given a priori. The latter varies in time, according to the ADN paradigm.

While the instantaneous degree distribution of the ADN is difficult to infer, similar to [8] its time integral over a prescribed window shares similarities with the distribution of the activity potential. To support this claim, we consider the union of consecutive realization of the ADN over a time span T, that is, $\cup_{t=0}^{T} G^t_{\mathrm{ADN}}$ [53]. We indicate the degree distribution of the obtained network with $P^{\mathrm{int}}(\mathrm{E}[k^T_{\mathrm{ADN}}])$, where k^T_{ADN} represents the degree of the integrated network. For a small window T compared to the network size, $T/N \ll 1$, we find that such a distribution is described by a power law with the same exponent of the activity

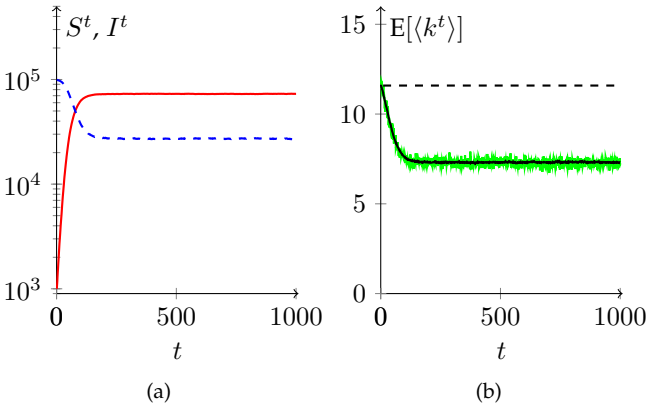

Fig. 2. Single realization of an SIS process on an ER backbone with ADN in the presence of individual behavioral changes. Panel (a): time evolution of the number of nodes in the susceptible and infected states (solid red line and blue dashed line, respectively). Panel (b): time evolution of the average degree in the network (green solid line) and expected average degree (black solid line), computed according to Eq. (1). The black dashed line represents the expected average degree for the ADN with no behavioral change and an ER static backbone. We choose $\eta = \eta_S$, such that $\mathrm{E}[\langle k^t\rangle] = 2\eta_S m\langle\alpha\rangle$. Parameter values are: $N = 10^5$, $\epsilon = 10^{-3}$, $\gamma = 2.1$, $\eta_I = 3$, $\eta_S = 15$, $m = 600$, $\langle k_{\mathrm{st}}\rangle = 5$, $\lambda = 0.01$, and $\mu = 0.015$. The fraction of random initial infected individuals is set to $0.01N$.

distribution (see the Appendix for a detailed derivation), that is,

$$P^{\mathrm{int}}(\mathrm{E}[k^T_{\mathrm{ADN}}]) \sim F\left(\xi\right). \tag{3}$$

The parameter ξ depends on the epidemic model studied. For example, in an SIS model, ξ takes the following form:

$$\xi = \frac{\mathrm{E}[k^T_{\mathrm{ADN}}]}{m\left(\eta_S T_S + \eta_I T_I\right)}, \tag{4}$$

where T_S, and T_I are the time spent (over the total aggregation time T) in states S and I, respectively, by a node with a degree k^T_{ADN} after T aggregations of the network of contacts. Since the total integration time is the same for all nodes, we must apply the closure relation: $T_S + T_I = T$. If no behavioral change is considered, $\eta_S = \eta_I = \eta$, we recover the same result as in [8], namely, $P^{\mathrm{int}}(\mathrm{E}[k^T_{\mathrm{ADN}}]) \sim F\left[\mathrm{E}[k^T_{\mathrm{ADN}}]/(m\eta T)\right]$. A similar expression for SIR models is obtained in the Appendix. Therefore, in both SIS and SIR epidemic processes, the time-varying links present a heavy tailed distribution, which is critical to model many real systems.

4 Analytical Computation of the Epidemic Threshold

The inclusion of behavioral changes and the analysis of RR backbones offer two significant improvements of the findings in [19] toward the study of realistic scenarios. For example, behavioral changes have been shown to be important in predicting the Ebola outbreak in 2014 [21], while RR backbones constitute a more plausible description of network resilience in real systems than ER networks [41], [54], [55], [56].

To disentangle the effect of these key improvements, we follow a sequential approach. First, we examine the effect of behavioral changes with an ER backbone. We present

analytical results for the epidemic threshold for both SIS and SIR processes. Second, we extend the approach to RR backbones with a narrow degree distribution or with a power law with cut-offs. We focus our analytical study on the SIS model.

4.1 Behavioral changes on ER backbones

For large N, we define R_α^t and I_α^t as the number of recovered and infected individuals in the network G^t with activity potential α at time t, respectively. Since the activity potential does not change in time, N_α is a constant quantity that represents the total number of individuals with activity potential α.

For an SIR model, the number of infected individuals in the network G^t with activity potential α at time $t+\Delta t$ is given by

$$\begin{aligned} I_\alpha^{t+\Delta t} =& I_\alpha^t - \mu \Delta t I_\alpha^t \\ &+ \lambda \left(N_\alpha - I_\alpha^t - R_\alpha^t\right) m \eta_S \alpha \Delta t \int d\alpha' \frac{I_{\alpha'}^t}{N} \\ &+ \lambda \left(N_\alpha - I_\alpha^t - R_\alpha^t\right) \int d\alpha' \frac{m \eta_I \alpha' \Delta t I_{\alpha'}^t}{N} \\ &+ \lambda \Delta t \langle k_{\rm st} \rangle I_\alpha^t. \end{aligned} \tag{5}$$

The first term on the right-hand side of Eq. (5) quantifies the number of infected individuals at the previous time step. The second term is the number of infected individuals who recover in the time interval Δt. The third and the fourth terms pertain to the dynamics of ADNs with behavioral change. More specifically, the third term represents active susceptible individuals in class α, respectively, active susceptible individuals in class α who become infected from any other infected individual with whom they connect via time-varying link. The fourth term describes any susceptible individual in class α, either active or not, who contracts the infection from any active infected individual via a time-varying link. The last term pertains to the ER static backbone, thereby quantifying new infections generated when infected nodes with activity potential α connect with other nodes via static links [20], [44], [57].

As detailed in the Appendix, an auxiliary equation is needed to compute the epidemic threshold. Such an equation is obtained by multiplying both sides of Eq. (5) by α. For both Eq. (5) and the auxiliary equation, we integrate over α, take the limit as $\Delta t \to 0$, and retain only the first-order terms. Through these steps, we ultimately obtain the following system of equations:

$$\begin{cases} \partial_t I = \left[-\mu + \lambda m \eta_S \langle \alpha \rangle + \lambda \langle k_{\rm st} \rangle\right] I + \lambda m \eta_I \theta \\ \partial_t \theta = \left[\lambda m \eta_S \langle \alpha^2 \rangle + \lambda \langle k_{\rm st} \rangle \langle \alpha \rangle\right] I + \left[-\mu + \lambda m \eta_I \langle \alpha \rangle\right] \theta \end{cases}, \tag{6}$$

where $I^t = \int d\alpha I_\alpha^t$ and $\theta^t = \int d\alpha I_\alpha^t \alpha$. Note that Eq. (6) is independent of the number of recovered nodes and the behavioral coefficient η_R. Eq. (6) applies to both SIS and SIR processes, as one may verify through equivalent calculations. Similar to [7], [8], [9], [14], [58], [59], the epidemic threshold is derived through a local stability analysis of Eq. (6) about the origin, which yields the following epidemic threshold:

$$\sigma = \left(\frac{\lambda}{\mu}\right)_{\rm threshold} = \frac{2}{\langle k_{\rm st} \rangle + m\left(\eta_S + \eta_I\right)\langle \alpha \rangle + \sqrt{\langle k_{\rm st} \rangle^2 + 2\langle k_{\rm st} \rangle m \left(\eta_S + \eta_I\right)\langle \alpha \rangle + m^2 \left[\left(\eta_I - \eta_S\right)^2 \langle \alpha \rangle^2 + 4\eta_S \eta_I \langle \alpha^2 \rangle\right]}}. \tag{7}$$

In agreement with our intuition, Eq. (7) posits that the epidemic threshold decreases with the average degree of the backbone, $\langle k_{\rm st} \rangle$, and the number of links generated by the active nodes in the ADN, m. As m approaches $N-1$ or $\langle k_{\rm st} \rangle$ approaches $N-1$, in the thermodynamic limit the epidemic threshold vanishes.

Eq. (7) generalizes previous results in the literature [7], [8], [20], [57]. In the absence of behavioral changes, $\eta_I = \eta_S = \eta$, we recover the threshold in [20]

$$\sigma = \frac{2}{\langle k_{\rm st} \rangle + 2m\langle a \rangle + \sqrt{\langle k_{\rm st} \rangle^2 + 4\langle k_{\rm st} \rangle m \langle a \rangle + 4m^2 \langle a \rangle}}. \tag{8}$$

For $m = 0$, this reduces to the classical threshold for ER networks, namely, $1/\langle k_{\rm st} \rangle$ [57]. Similarly, in the absence of the static backbone, $\langle k_{\rm st} \rangle = 0$, we recover the prediction in [7]

$$\sigma = \frac{2}{m\left[\left(\eta_S + \eta_I\right)\langle \alpha \rangle + \sqrt{\left(\eta_I - \eta_S\right)^2 \langle \alpha \rangle^2 + 4\eta_S \eta_I \langle \alpha^2 \rangle}\right]}. \tag{9}$$

The threshold in [8] can be easily recovered from either of Eqs. (8) or (9), by setting $\langle k_{\rm st} \rangle = 0$ or $\eta_I = \eta_S = \eta$, respectively.

4.2 Behavioral changes on RR backbones

To tackle RR networks, we apply the classical method of homogeneous pair approximation [60], which finds application in network science to account for the presence of pairs of connected and infected nodes in the static backbone [44]. The homogeneous pair approximation only considers interactions between nodes of the same degree, in contrast to more refined heterogeneous pair approximations [43], [45]. However, the increase in computational complexity to deal with heterogeneous interactions has not been shown to translate into improved estimates [45].

We define u^t as the probability of having a pair of connected and infected nodes at time t in the static backbone, $N_\alpha u^t$ as the expected number of pairs within the class of activity α, and $U^t = N u^t$ as the expected total number of pairs. The SIR model may not be treated with

a homogeneous pair approximation, because nodes can also be immunized [50], [61], [62]; the numerical study of an SIR process is addressed in the following Section. For an SIS model, the number of infected individuals in with activity potential α at time $t+\Delta t$ is given by (details in the Appendix)

$$\begin{aligned} I_{\alpha}^{t+\Delta t} =& I_{\alpha}^{t} - \mu \Delta t I_{\alpha}^{t} + \lambda \left(N_{\alpha} - I_{\alpha}^{t}\right) m \eta_S \alpha \Delta t \int d\alpha' \frac{I_{\alpha'}^{t}}{N} \\ &+ \lambda \left(N_{\alpha} - I_{\alpha}^{t}\right) \int d\alpha' \frac{m \eta_I \alpha' \Delta t I_{\alpha'}^{t}}{N} \\ &+ \lambda \Delta t k_{\mathrm{st}} I_{\alpha}^{t} - \lambda \Delta t k_{\mathrm{st}} N_{\alpha} u^{t}. \end{aligned} \tag{10}$$

Eq. (10) is equivalent to Eq. (5), with the exception of the last term, introduced by the pair approximation. The last two terms in Eq. (10) summarize the "net" available connections for the disease to spread in the network, by measuring the difference between the number of links with one end infected and the number of links with both ends infected. Insight into the basis for this approximation can be found in the Appendix of [44]. Note that the number of pairs in the ADN is neglected in our treatment, since the ADN leads to a random uncorrelated network.

A mean-field argument similar to the one applied to Eq. (6) leads to the following system of equations:

$$\begin{cases} \partial_t I = \left[-\mu + \lambda m \eta_S \langle \alpha \rangle + \lambda k_{\mathrm{st}}\right] I + \lambda m \eta_I \theta - \lambda k_{\mathrm{st}} U \\ \partial_t \theta = \left[\lambda m \eta_S \langle \alpha^2 \rangle + \lambda k_{\mathrm{st}} \langle \alpha \rangle\right] I + \left[-\mu + \lambda m \eta_I \langle \alpha \rangle\right] \theta - \lambda k_{\mathrm{st}} \langle \alpha \rangle U \\ \partial_t U = \lambda k_{\mathrm{st}} I + \left[-\mu k_{\mathrm{st}} - \lambda k_{\mathrm{st}}\right] U. \end{cases} \tag{11}$$

Comparing the first two equations in Eq. (11) with Eq. (6), we note the presence of an additional summand that is associated with the pair approximation in Eq. (11) that cogently determines the evolution of the number of pairs in the backbone only.

We were not able to derive a compact, closed-form expression for the threshold for any choice of model parameters. However, in some special cases, it is possible to derive elegant expressions. For example, for $m = 0$, we recover $\sigma = 1/(k_{\mathrm{st}} - 1)$, in agreement with [44]. In general, it is possible to solve the steady state numerically by considering the largest fixed point solution, following [44], [57].

5 Analytical and Numerical Results

To evaluate the SIS and SIR thresholds numerically, we follow the methods proposed in [50], [51], [63]. Further details about the procedure adopted can be found in the Appendix. Without loss of generality, in the numerical computation, we set $\Delta t = 1$ and, for an SIR model, $\eta_R = 0$. The aim of this Section is two-fold. First, we validate our theoretical approach through extensive numerical simulations. Second, we assess the effect of model parameters on the epidemic threshold. We compare our results with findings from [7], [20], which contain specializations of our claims.

In Fig. 3, we analyze epidemic spreading for SIS and SIR models in the presence of behavioral changes for either ER or RR backbones. By comparing theoretical predictions from Eq. (7) with numerical findings, we confirm the validity of a common mean-field approximation to infer the epidemic threshold of both SIS and SIR models for ER and RR static backbones. Relative differences between numerical findings and theoretical predictions are in the range of 0.02 for a range of values of η_I/η_S from 0 to 1. In general, predictions on the SIS model tend to yield relative errors of 0.02, while predictions on SIR reach a higher value of 0.05. Thus, our mean-field approximation is successful in anticipating a decrease in the resilience of the network to the disease for increasing values of η_I/η_S. Increasing the value

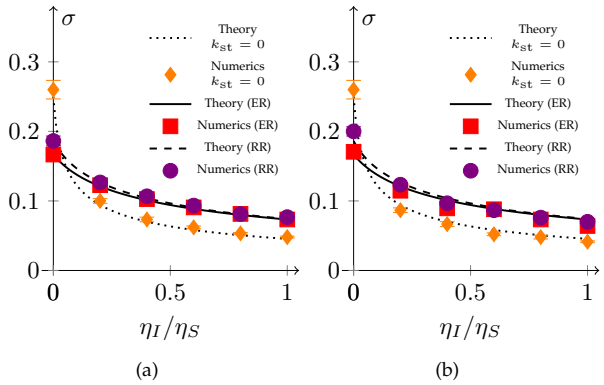

Fig. 3. Epidemic threshold for ER and RR backbones ($\langle k_{\mathrm{st}} \rangle = 4$ and $m = 364$), along with pure ADN ($\langle k_{\mathrm{st}} \rangle = 0$ and $m = 728$) as functions of η_I/η_S. The theoretical predictions from Eqs. (7) and (9) are plotted with solid and dotted lines, respectively. The dashed line represents the theoretical prediction from the linear stability analysis in Eq. (11). Markers are used to label numerical results. Panel (a): SIS model, and panel (b): SIR models. We set $\eta_S = 15$ and let η_I varies: $0 \leq \eta_I \leq \eta_S$. Parameter values are: $N = 10^5$, $T = 10^5$, $\epsilon = 10^{-3}$, $\gamma = 2.1$, and $\mu = 0.015$. For the numerical computations, data are reported as medians of 10^2 independent simulations for the SIS model and 10^3 for the SIR model. The fraction of random initial infected individuals is set to $0.01N$. Vertical lines indicate 95% confidence intervals, although not always visible.

of η_I/η_S implies that individuals maintain a high activity upon infection, thereby facilitating the spread and lowering the threshold.

In addition to numerical validation, Fig. 3 offers a comparative assessment of the role of the static backbone network. Specifically, we include numerical findings and theoretical predictions for a pure ADN, in which the backbone is omitted. To afford a meaningful assessment of the static backbone, we initialize the simulations to match the expected average degree. We reiterate the accuracy of Eq. (9) against numerics, as already shown in our previous work [21].

From such a comparative assessment, we uncover a

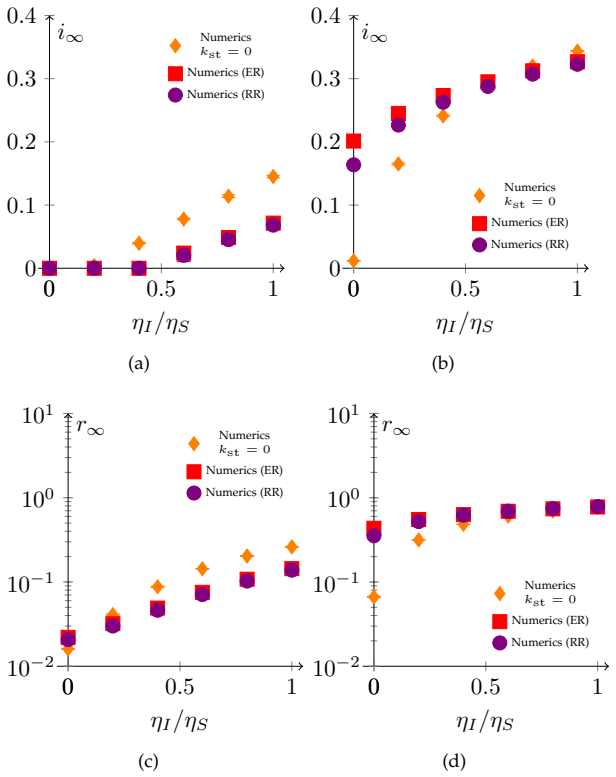

Fig. 4. Epidemic size for ER and RR backbones ($\langle k_{st}\rangle = 4$ and $m = 364$), along with pure ADN ($\langle k_{st}\rangle = 0$ and $m = 728$) as functions of η_I/η_S. i_∞ and r_∞ represent the fractions of infected and recovered nodes at the end of the simulation, respectively. Panel (a): SIS model with $\lambda/\mu = 0.1$. Panel (b): SIS model with $\lambda/\mu = 0.3$. Panel (c): SIR model with $\lambda/\mu = 0.1$. Panel (d): SIR model with $\lambda/\mu = 0.3$. We set $\eta_S = 15$ and let η_I varies: $0 \leq \eta_I \leq \eta_S$. Parameter values are: $N = 10^5$,$T = 10^5$, $\epsilon = 10^{-3}$, $\gamma = 2.1$, and $\mu = 0.015$. For the numerical computations, data are reported as medians of 10^2 independent simulations for the SIS model and 10^3 for the SIR model. The fraction of random initial infected individuals is set to $0.01N$. Vertical lines indicate 95% confidence intervals, although not always visible.

non-monotonic relationship between the thresholds of the two models, with and without the static backbone. More specifically, the two thresholds cross over at a certain value of η_I/η_S, approximately at $\eta_I/\eta_S = 0.05$, independent of the type of static backbone, ER or RR. When the behavioral effect is dominant (small η_I/η_S), the presence of the static backbone reduces the resilience of the network, while for weaker behavioral changes, we observe an improvement due to the presence of the backbone. This phenomenon should be ascribed to the interplay between two competing effects. On the one hand, the ADN causes a heterogeneous degree distribution, in an integral sense, as shown in Eq. (3), which lowers the epidemic threshold. On the other, small values of η_I/η_S reduce the effectiveness of the ADN in supporting the disease spreading, whereby infected individuals will tend to establish fewer connections with susceptible individuals through the ADN. Overall, this comparison suggests that static connections tend to improve the network resilience, except when the disease will cause drastic activity reductions. In this case, the disease will not propagate through time-varying links, but only through static ones, associated with family members and close friends.

To delve more on the role of behavioral changes on epidemic spreading, in Fig. 4 we report numerical results on the epidemic size for both SIS and SIR models. More specifically, for the SIS model, we report the fraction of infected individuals at steady state and for the SIR model, we concentrate on the steady state fraction of recovered individuals, which amounts to the total number of infections throughout the duration of the simulation. We consider two different values of the ratio λ/μ, that is, 0.3 and 0.1, exemplifying two complementary conditions, as shown in Fig. 3. $\lambda/\mu = 0.3$ is always above the epidemic threshold irrespective of the value of η_I/η_S. This condition leads to the inception of the epidemic spreading, irrespective of the intensity of behavioral changes. On the other hand, the value of η_I/η_S determines whether $\lambda/\mu = 0.1$ is below or above the epidemic threshold, such that behavioral changes have a critical role on the onset of the epidemic spreading.

Fig. 4(a) confirms that for sufficiently small values of η_I/η_S, an epidemic-free state is achieved for the SIS model. In agreement with our intuition, above the epidemic threshold, the presence of a static backbone mitigates the severity of the infection. Increasing the value of λ/μ to 0.3 systematically leads to an epidemic state, in which the fraction of infected individuals depends on both the static backbone and the value of η_I/η_S. Similar to Fig. 3, we discover the existence of a cross over phenomenon, where for small values of η_I/η_S, the backbone has a detrimental role on the epidemics, while for large values, it improves the network propensity to stop the inception of the epidemic spreading. Interestingly, the numerical value of η_I/η_S at which the cross over occurs if the size of the epidemic is above 0.5, in contrast with observations in Fig. 3 on the epidemic threshold. Results on the SIR model in Figs. 4(c) and (d) echo these findings, by pointing at a complex interplay between the static backbone and behavioral changes in shaping the epidemic size of the network.

We consider two widely different instances of the ADN model, such that $m = 2$ and 364. In Fig. 5, we confirm an excellent agreement between theoretical and numerical predictions for both SIS and SIR models for any selection of the average static degree and both the choices of m. The prediction of the epidemic threshold for the SIS model from Eq. (11) based on the homogeneous pair approximation is also in very good agreement with numerical results. For ER backbones, we find that the epidemic threshold decreases with the average static degree for both the selections of m, similar to what is claimed in [20]. However, due to the presence of behavioral effects we register an increase in the epidemic threshold. Inspection of results for RR backbones, displays an equivalent dependence on the static degree, with network resilience decreasing with the degree of the static backbone.

Comparing the epidemic thresholds for ER and RR backbones, we determine a meaningful difference only for $m = 2$, whereby for small values of the average static degree RR backbones show a higher epidemic threshold. This phenomenon should be ascribed to the fact that the two static networks have different epidemic thresholds for the same average degree, namely, $\sigma = 1/\langle k_{st}\rangle$ and $\sigma = 1/(k_{st} - 1)$ for ER and RR networks, respectively. For $m = 2$, the relative weight of the static backbone is larger, such that the different response of ER and RR backbones can be appreciated. On

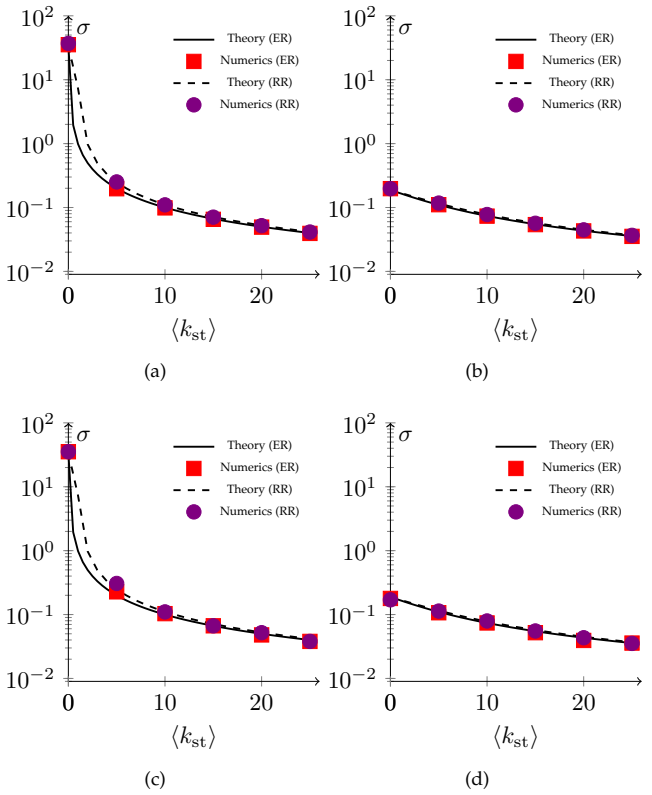

Fig. 5. Epidemic thresholds for ER and RR backbones as a functions of the average static degree $\langle k_{st} \rangle$; for RR backbones the average degree is equal to the actual degree. The theoretical prediction from Eq. (7) is plotted with solid line. The dashed line represents the theoretical prediction from the linear stability analysis in Eq. (11). Markers are used to label numerical results. Panel (a): SIS model and $m = 2$; Panel (b): SIS model and $m = 364$; Panel (c): SIR model and $m = 2$; and Panel (d): SIR model and $m = 364$. Parameter values are: $N = 10^5$, $T = 10^5$, $\epsilon = 10^{-3}$, $\gamma = 2.1$, $\mu = 0.015$, $\eta_I = 3$, and $\eta_S = 15$. For the numerical computations, data are reported as medians of 10^2 independent simulations for the SIS model, and 10^3 for the SIR model. The fraction of random initial infected individuals is set to $0.01N$. Vertical lines indicate 95% confidence intervals, although not always visible.

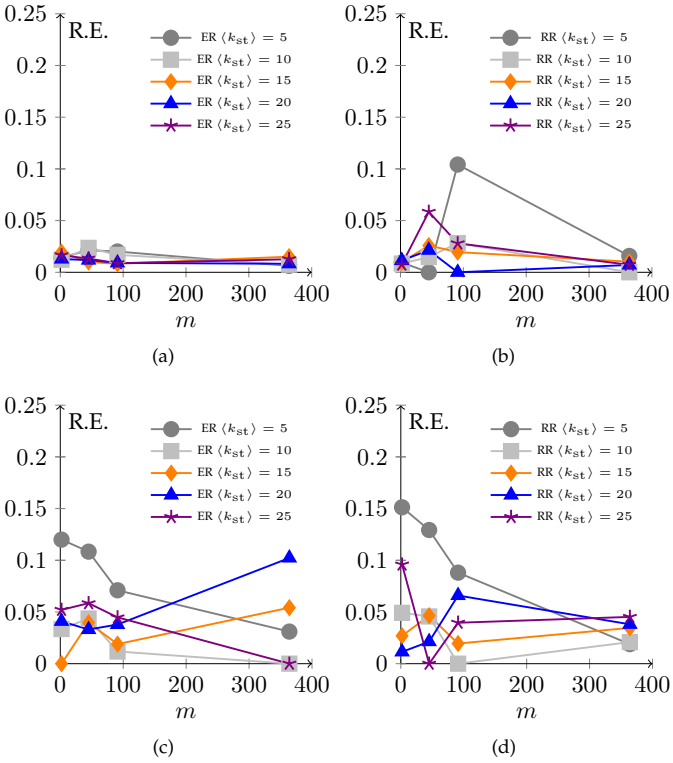

Fig. 6. Relative error (R.E.) between theoretical predictions and simulation thresholds as a function of m, for five values of the average degree of the static backbone, $\langle k_{st} \rangle$. Panel (a): SIS model and ER backbone. Panel (b): SIS model and RR backbone. Panel (c): SIR model and ER backbone. Panel (d): SIR model and RR backbone. For panels (a) and (c), Eq. (7) is used for theoretical predictions, while for panels (b) and (d), theoretical predictions are associated with the stability analysis of the system in Eq. (11). Parameter values are: $N = 10^5$, $T = 10^5$, $\epsilon = 10^{-3}$, $\gamma = 2.1$, $\mu = 0.015$, $\eta_I = 3$, and $\eta_S = 15$. For the numerical computations, data are reported as medians of 10^2 independent simulations for the SIS model, and 10^3 for the SIR model. The fraction of random initial infected individuals is set to $0.01N$.

the other hand, for $m = 364$, these differences are masked by the dominant effect of the ADN. Therefore, for large values of m, an equivalent behavior should be expected from ER and RR backbones, such that Eq. (7) could be applied in both cases without the need of tracking the number of pairs in the network.

Figs. 3 and 5 offer compelling evidence for the accuracy of our theoretical estimate of the epidemic threshold, yet they focus on either values of m close to 1 or of several hundreds. To investigate the accuracy of our theoretical findings for intermediate values of m, in Fig. 6, we report the relative error (R.E.) between theoretical predictions and numerical simulations for both SIS and SIR models for four different values of m, including 2, 45, 91, and 364. The comparison is carried out for both ER and RR networks, spanning five different values of $\langle k_{st} \rangle$, from 5 to 25 in increments of 5. In agreement with our expectations, theoretical predictions are more accurate for the SIS than for the SIR model. For most of the combinations, the relative error is less than 0.05 for the SIS model, while we register larger errors up to 0.15 for the SIR model. It is difficult to tease out a dependence of the relative error on either the average degree of the static backbone or the value of m.

6 Discussion and Conclusion

ADNs have emerged as the paradigm of choice when studying epidemic processes over temporal networks, in which the evolution of the links and the disease share a common time-scale. Although the potential of ADN has been acknowledged by a number of technical publications, the lack of preferential connections among individuals constitutes a major methodological drawback of this modeling approach. In this paper, we have sought to bridge this gap within an improved modeling framework that superimposes the intermittent contacts generated by ADNs with persistent links of a static backbone network.

The proposed modeling framework is inspired by recent findings in [20], which we extend along two main research directions. First, we propose an adaptive mechanism that encapsulates behavioral changes of individuals associated with their health status. By including a set of behavioral coefficients, we enable the study of the coupled evolution of the links and the disease, contrasting the classical ADN

formulation, where links are generated independently of the disease. Second, we expand on the range of static backbones to account for random regular networks, which constitute a significant improvement in the study of realistic epidemic processes. This extension involves the implementation of a more sophisticated mean-field approach, relying on homogeneous pair approximation. From a theoretical point of view, we demonstrate that behavioral changes have a critical role on topological properties of the network of contacts, by regulating the interplay between the static backbone and the time-varying topology of the ADN. In the thermodynamic limit, we establish a systematic procedure for quantifying the role of behavioral changes on the instantaneous average degree and the degree distribution of a time-integrated network, summarizing the evolution of the network of contacts over a finite window.

By focusing on SIS and SIR models, we establish an accurate mean-field theory to predict the epidemic threshold for both ER and RR networks. With respect to ER networks, our approach naturally extends findings reported in [20] to account for behavioral changes; while a different methodology is required for tackling RR networks. Through a homogeneous pair approximation, we lay the foundation of a mean-field analysis of realistic ADN models where it is crucial to specifically track the number of pairs of active nodes at each time. Notably, when specialized to known instances in the technical literature, our approach is successful in retrieving existing closed-form results.

Through comparison with numerical simulations, we demonstrate the accuracy of our theoretical predictions and their value in providing powerful insight into the disease dynamics. Our results point at a rich, nontrivial interaction between static links, time-varying connections, and behavioral changes in shaping the resilience of the network to a disease outbreak, scored in terms of the epidemic threshold and epidemic size. When the infection elicits a strong reduction of individual activity, the presence of the static backbone decreases the resilience of the network, because an infected individual remains confined in his/her social circle of strong ties, thereby promoting the formation of local communities of infected individuals. On the other hand, when behavioral changes have a modest effect on activity, the presence of a static backbone improves the resilience of the network to the epidemic spreading, by hampering the long-range mixing process supported by the ADN. While ER and RR backbones exhibit a comparable response for dense ADNs, remarkable differences are observed for sparse ADNs, where RR backbones yields improved resilience.

Although the proposed modeling framework constitutes a significant technical advancement from a theoretical point of view, its methodological premise warrants further consideration. More specifically, the feasibility of enforcing a distinct separation between a static backbone and an intermittent ADN needs to be thoroughly tested on real-world data. We envision two parallel lines of research toward this ambitious goal. First, hypothesis-driven experiments should be designed on small populations to generate spatially and temporally refined datasets to support empirical validation. Second, future work should focus on establishing reliable methodologies to infer general time-varying topologies from sparse data on large populations, thereby allowing for the precise estimation of static versus intermittent links.

Acknowledgements

The authors acknowledges financial support from the National Science Foundation under grant No. CMMI-1561134 and the Army Research Office under grant No. W911NF-15-1-0267, with Drs A. Garcia and S.C. Stanton as program managers. A.R. acknowledges financial support from Compagnia di San Paolo, Italy. Also, the authors would like to express their gratitude to anonymous reviewers, whose constructive feedback has helped improve the work and its presentation.

Authors' contribution

A.R. and M.P. formulated the research questions. M.N. performed the numerical simulations, developed the analytical treatment, and wrote a first draft of the manuscript. All the authors contributed to mathematical analysis and discussed the results. A.R. and M.P. wrote the paper in its final form.

References

[1] P. Holme and J. Saramäki, "Temporal networks," *Physics Reports*, vol. 519, no. 3, pp. 97–125, 2012.

[2] I. Belykh, M. Di Bernardo, J. Kurths, and M. Porfiri, "Evolving dynamical networks," *Physica D: Nonlinear Phenomena*, vol. 267, pp. 1–6, 2014.

[3] K. Dietz, "On the transmission dynamics of hiv," *Mathematical Biosciences*, vol. 90, no. 1-2, pp. 397–414, 1988.

[4] C. Watts and R. May, "The influence of concurrent partnerships on the dynamics of HIV/AIDS," *Mathematical biosciences*, vol. 108, no. 1, pp. 89–104, 1992.

[5] M. Kretzschmar and M. Morris, "Measures of concurrency in networks and the spread of infectious disease," *Mathematical biosciences*, vol. 133, no. 2, pp. 165–195, 1996.

[6] N. Masuda and P. Holme, *Temporal Network Epidemiology*, 1st ed., ser. Theoretical Biology. Springer Singapore, 2017.

[7] A. Rizzo, M. Frasca, and M. Porfiri, "Effect of individual behavior on epidemic spreading in activity driven networks," *Physical Review E*, vol. 90, p. 042801, 2014.

[8] N. Perra, B. Gonçalves, R. Pastor-Satorras, and A. Vespignani, "Activity driven modeling of time varying networks." *Scientific Reports*, vol. 2, p. 469, 2012.

[9] S. Liu, N. Perra, M. Karsai, and A. Vespignani, "Controlling contagion processes in activity driven networks," *Physical Review Letters*, vol. 112, p. 118702, 2014.

[10] A. Rizzo and M. Porfiri, "Innovation diffusion on time-varying activity driven networks," *The European Physical Journal B*, vol. 89, no. 1, pp. 1–8, 2016.

[11] C. Liu, L.-X. Zhou, C.-J. Fan, L.-A. Huo, and Z.-W. Tian, "Activity of nodes reshapes the critical threshold of spreading dynamics in complex networks," *Physica A: Statistical Mechanics and its Applications*, vol. 432, pp. 269–278, 2015.

[12] Y. Zou, W. Deng, W. Li, and X. Cai, "A study of epidemic spreading on activity-driven networks," *International Journal of Modern Physics C*, vol. 27, no. 08, p. 1650090, 2016.

[13] M. Starnini and R. Pastor-Satorras, "Temporal percolation in activity-driven networks," *Physical Review E*, vol. 89, no. 3, p. 032807, 2014.

[14] L. Zino, A. Rizzo, and M. Porfiri, "Continuous-time discrete-distribution theory for activity-driven networks," *Physical Review Letters*, vol. 117, p. 228302, Nov 2016.

[15] ——, "An analytical framework for the study of epidemic models on activity driven networks," *Journal of Complex Networks*, vol. 5, no. 6, pp. 924–952, 2017.

[16] R. Yulmetyev, N. Emelyanova, S. Demin, F. Gafarov, P. Hänggi, and D. Yulmetyeva, "Non-markov stochastic dynamics of real epidemic process of respiratory infections," *Physica A: Statistical Mechanics and its Applications*, vol. 331, no. 1-2, pp. 300–318, 2004.

[17] T. Liu, P. Li, Y. Chen, and J. Zhang, "Community size effects on epidemic spreading in multiplex social networks," *PLoS ONE*, vol. 11, no. 3, p. e0152021, 2016.

[18] K. Sun, A. Baronchelli, and N. Perra, "Contrasting effects of strong ties on sir and sis processes in temporal networks," *The European Physical Journal B*, vol. 88, no. 12, pp. 1–8, 2015.

[19] M.-X. Liu, W. Wang, Y. Liu, M. Tang, S.-M. Cai, and H.-F. Zhang, "Social contagions on time-varying community networks," *Physical Review E*, vol. 95, no. 5, p. 052306, may 2017.

[20] Y. Lei, X. Jiang, Q. Guo, Y. Ma, M. Li, and Z. Zheng, "Contagion processes on the static and activity-driven coupling networks," *Physical Review E*, vol. 93, p. 032308, Mar 2016.

[21] A. Rizzo, B. Pedalino, and M. Porfiri, "A network model for ebola spreading," *Journal of Theoretical Biology*, vol. 394, pp. 212 – 222, 2016.

[22] M. S. Granovetter, "The strength of weak ties," in *Social Networks*. Elsevier, 1977, pp. 347–367.

[23] E. Gilbert and K. Karahalios, "Predicting tie strength with social media," in *Proceedings of the SIGCHI Conference on Human Factors in Computing Systems*, ser. CHI '09. New York, NY, USA: ACM, 2009, pp. 211–220.

[24] J.-P. Onnela, J. Saramäki, J. Hyvönen, G. Szabó, D. Lazer, K. Kaski, J. Kertész, and A.-L. Barabási, "Structure and tie strengths in mobile communication networks," *Proceedings of the National Academy of Sciences*, vol. 104, no. 18, pp. 7332–7336, 2007.

[25] M. Karsai, N. Perra, and A. Vespignani, "Time varying networks and the weakness of strong ties," *Scientific Reports*, vol. 4, p. 4001, 2014.

[26] G. Krings, M. Karsai, S. Bernhardsson, V. D. Blondel, and J. Saramäki, "Effects of time window size and placement on the structure of an aggregated communication network," *EPJ Data Science*, vol. 1, no. 1, p. 4, 2012.

[27] P. Shu, M. Tang, K. Gong, and Y. Liu, "Effects of weak ties on epidemic predictability on community networks," *Chaos: An Interdisciplinary Journal of Nonlinear Science*, vol. 22, no. 4, p. 043124, 2012.

[28] E. Huszti, B. Dávid, and K. Vajda, "Strong tie, weak tie and in-betweens: A continuous measure of tie strength based on contact diary datasets," *Procedia - Social and Behavioral Sciences*, vol. 79, pp. 38 – 61, 2013, 9th Conference on Applications of Social Network Analysis (ASNA).

[29] M. Karsai, N. Perra, and A. Vespignani, "Time varying networks and the weakness of strong ties," *Scientific Reports*, vol. 4, 2014.

[30] M. Nadini, K. Sun, E. Ubaldi, M. Starnini, A. Rizzo, and N. Perra, "Epidemic spreading in modular time-varying networks," *Scientific Reports*, vol. 8, no. 1, p. 2352, 2018.

[31] J. M. Epstein, J. Parker, D. Cummings, and R. A. Hammond, "Coupled contagion dynamics of fear and disease: Mathematical and computational explorations," *PLoS One*, vol. 3, p. E3955, 2008.

[32] S. Funk, E. Gilad, C. Watkins, and V. A. A. Jansen, "The spread of awareness and its impact on epidemic outbreaks." *Proceedings of the National Academy of Sciences*, vol. 106, no. 16, pp. 6872–7, 2009.

[33] P. Poletti, B. Caprilea, M. Ajelli, A. Pugliese, and S. Merler, "Spontaneous behavioural changes in response to epidemics," *Journal of Theoretical Biology*, vol. 260, p. 31, 2009.

[34] E. P. Fenichel, C. Castillo-Chavez, M. G. Ceddia, G. Chowell, P. A. G. Parra, G. J. Hickling, G. Holloway, R. Horan, B. Morin, C. Perrings, M. Springborn, L. Velazquez, and C. Villalobos, "Adaptive human behavior in epidemiological models," *Proceedings of the National Academy of Sciences*, vol. 108, no. 15, p. 6306, Apr. 2011.

[35] F. D. Sahneh, J. Melander, C. Scoglio *et al.*, "Contact adaption during epidemics: A multilayer network formulation approach," *IEEE Transactions on Network Science and Engineering*, 2017.

[36] G. Chowell, P. W. Fenimore, M. A. Castillo-Garsow, and C. Castillo-Chavez, "SARS outbreak in Ontario, Hong Kong and Singapore: the role of diagnosis and isolation as a control mechanism," *Journal of Theoretical Biology*, vol. 224, no. 1, pp. 1–8, 2003.

[37] L. S. Hung, "The SARS epidemic in Hong Kong: what lessons have we learned?" *Journal of The Royal Society of Medicine*, vol. 96, no. 8, pp. 374–378, 2003.

[38] S. Riley, C. Fraser, C. A. Donnelly, A. C. Ghani, L. J. Abu-Raddad, A. J. Hedley, G. M. Leung, L. M. Ho, T. H. Lam, T. Q. Thach *et al.*, "Transmission dynamics of the etiological agent of SARS in Hong Kong: impact of public health interventions," *Science*, vol. 300, no. 5627, pp. 1961–1966, 2003.

[39] M. Cotten, S. J. Watson, and A. I. Zumla, "Spread, circulation, and evolution of the Middle East respiratory syndrome coronavirus," *MBio*, vol. 5, no. 1, pp. e01 062–13, 2014.

[40] P. Erdös and A. Rényi, "On random graphs, I," *Publicationes Mathematicae (Debrecen)*, vol. 6, pp. 290–297, 1959.

[41] M. Newman, D. Watts, and S. Strogatz, "Random graph models of social networks," *Proceedings of the National Academy of Sciences*, vol. 99, no. suppl 1, pp. 2566–2572, 2002.

[42] I. Kiss, J. Miller, and P. Simon, *Mathematics of Epidemics on Networks*. Springer, 2017.

[43] S. Ferreira, R. Ferreira, C. Castellano, and R. Pastor-Satorras, "Quasistationary simulations of the contact process on quenched networks," *Physical Review E*, vol. 84, no. 6, p. 066102, Dec. 2011.

[44] R. Juhász, G. Ódor, C. Castellano, and M. A. Munoz, "Rare-region effects in the contact process on networks," *Physical Review E*, vol. 85, no. 6, p. 066125, 2012.

[45] A. S. Mata, R. S. Ferreira, and S. C. Ferreira, "Heterogeneous pair-approximation for the contact process on complex networks," *New Journal of Physics*, vol. 16, no. 5, p. 053006, 2014.

[46] M. J. Keeling and P. Rohani, *Modeling Infectious Diseases in Humans and Animals*. Princeton University Press, 2007.

[47] S. Jack, "The Role, Use and Activation of Strong and Weak Network Ties: A Qualitative Analysis*," *Journal of Management Studies*, vol. 42, pp. 1233–1259, Sep. 2005.

[48] E. Demaine, F. Reidl, P. Rossmanith, F. Villaamil, S. Sikdar, and B. Sullivan, "Structural sparsity of complex networks: Bounded expansion in random models and real-world graphs," *arXiv preprint arXiv:1406.2587*, 2014.

[49] N. C. Wormald, "Models of random regular graphs," *London Mathematical Society Lecture Note Series*, pp. 239–298, 1999.

[50] C. Castellano and R. Pastor-Satorras, "On the numerical study of percolation and epidemic critical properties in networks," *The European Physical Journal B*, vol. 89, no. 11, 2016.

[51] A. Moinet, R. Pastor-Satorras, and A. Barrat, "Effect of risk perception on epidemic spreading in temporal networks," *Physical Review E*, vol. 97, no. 1, p. 012313, Jan. 2018.

[52] N. Perra, D. Balcan, B. Gonçalves, and A. Vespignani, "Towards a characterization of behavior-disease models," *PLoS ONE*, vol. 6, no. e23084, 2011.

[53] A. Bondy and M. R. Murty, *Graph Theory*. Springer, 2008.

[54] A.-L. Barabási and R. Albert, "Emergence of scaling in random networks," *Science*, vol. 286, no. 5439, pp. 509–512, 1999.

[55] M. E. J. Newman, *Networks: an introduction*. Oxford university press, 2010.

[56] A. L. Barabási, *Network Science*. Cambridge University Press, 2016.

[57] R. Pastor-Satorras and A. Vespignani, "Epidemic spreading in scale-free networks," *Physical Review Letters*, vol. 86, no. 14, pp. 3200–3203, Apr. 2001.

[58] S.-Y. Liu, A. Baronchelli, and N. Perra, "Contagion dynamics in time-varying metapopulation networks," *Physical Review E*, vol. 87, no. 3, p. 032805, 2013.

[59] I. Pozzana, K. Sun, and N. Perra, "Epidemic spreading on activity-driven networks with attractiveness," *Physical Review E*, vol. 96, no. 4, p. 042310, Oct. 2017.

[60] D. Rand, "Correlation equations and pair approximations for spatial ecologies," *Advanced ecological theory: principles and applications*, vol. 100, 1999.

[61] M. E. J. Newman, "Spread of epidemic disease on networks," *Physical Review E*, vol. 66, no. 1, p. 016128, Jul. 2002.

[62] R. Pastor-Satorras, C. Castellano, P. Van Mieghem, and A. Vespignani, "Epidemic processes in complex networks," *Reviews of Modern Physics*, vol. 87, no. 3, pp. 925–979, Aug. 2015.

[63] M. Boguñá, C. Castellano, and R. Pastor-Satorras, "Nature of the epidemic threshold for the susceptible-infected-susceptible dynamics in networks," *Physical Review Letters*, vol. 111, p. 068701, Aug 2013.

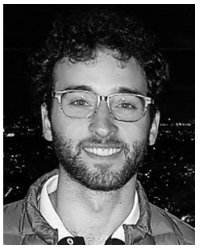

Matthieu Nadini Mr. Matthieu Nadini was born in Modena, Italy, in 1993. He received B.Sc. degree in Physics from University of Modena and Reggio Emilia in 2015, a M2R in Physics of Complex Systems from Paris Diderot University in 2017, and an M.Sc. in Physics of Complex Systems from Polytechnic University of Turin in 2017 (summa cum laude). Presently, he is a Ph.D. student at New York University, New York, NY, USA , jointly mentored by Profs. Porfiri and Rizzo. His research interests include network science, epidemiology, and computational social science.

Alessandro Rizzo Dr. Alessandro Rizzo is an Associate Professor in the Department of Electronics and Telecommunications at Politecnico di Torino, Italy. He received the “Laurea” degree (summa cum laude) in computer engineering and the Ph.D. degree in automation and electronics engineering from the University of Catania, Italy, in 1996, and 2000, respectively. In 1998, he worked as EURATOM Research Fellow at JET Joint Undertaking, Abingdon, U.K., researching on sensor validation and fault diagnosis for nuclear fusion experiments. In 2000 and 2001, he worked as Research Consultant to ST Microelectronics, Catania Site, Italy, and as Industry Professor of Robotics at the University of Messina, Italy. From 2002 to 2015 he was a tenured Assistant Professor at Politecnico di Bari, Italy. In November 2015, he joined Politecnico di Torino. From 2012, he has also been a Visiting Professor at New York University Tandon School of Engineering, Brooklyn NY, USA. Prof. Rizzo is engaged in conducting and supervising research on complex networks and systems, modeling and control of nonlinear systems, cooperative robotics. He is author of two books, two international patents, and more than 130 papers on international journals and conference proceedings. Prof. Rizzo has been the recipient of the award for the best application paper at the IFAC world triennial conference in 2002 and of the award for the most read papers in Mathematics and Computers in Simulation (Elsevier) in 2009. Prof. Rizzo is also a Distinguished Lecturer of the IEEE Nuclear and Plasma Science Society.

Maurizio Porfiri Dr. Maurizio Porfiri is a Professor in the Department of Mechanical and Aerospace Engineering at New York University Tandon School of Engineering. He received M.Sc. and Ph.D. degrees in Engineering Mechanics from Virginia Tech, in 2000 and 2006; a “Laurea” in Electrical Engineering (with honours) and a Ph.D. in Theoretical and Applied Mechanics from the University of Rome La Sapienza” and the University of Toulon (dual degree program), in 2001 and 2005, respectively. He is engaged in conducting and supervising research on dynamical systems theory, multiphysics modeling, and underwater robotics. Maurizio Porfiri is the author of more than 250 journal publications and the recipient of the National Science Foundation CAREER award. He has been included in the “Brilliant 10” list of Popular Science and his research featured in all the major media outlets, including CNN, NPR, Scientific American, and Discovery Channel. Other significant recognitions include invitations to the Frontiers of Engineering Symposium and the Japan-America Frontiers of Engineering Symposium organized by National Academy of Engineering; the Outstanding Young Alumnus award by the college of Engineering of Virginia Tech; the ASME Gary Anderson Early Achievement Award; the ASME DSCD Young Investigator Award; and the ASME C.D. Mote, Jr. Early Career Award.

APPENDIX

Analytical derivation of the average degree and degree distribution

We derive closed-form expressions for the average degree and the degree distribution of the network of contacts, for an epidemic model with M discrete states $\mathcal{X} \triangleq \{x_1, \ldots, x_M\}$. The results for SIR and SIS models are obtained as particular cases.

First, we analytically compute the expected average degree of the time-varying links, $\mathrm{E}\left[k^t_{\mathrm{ADN}}\right]$. The expected total degree is then obtained by summing to this term the average degree of the static backbone, $\langle k_{\mathrm{st}} \rangle$. Here and in what follows, we introduce the following nomenclature. At each discrete time step, a node belongs to only one state j, defined as x_j. The behavioral coefficient for state x_j is η_{x_j}. The number of nodes with activity α which belongs to x_j at time t is indicated with $n^t_{x_j,\alpha}$. The total number of nodes with activity potential α at time t is $\sum_{j=1}^{M} n^t_{x_j,\alpha} = n^t_\alpha$. The total number of nodes in x_j at time t is $\int d\alpha\, n^t_{x_j,\alpha} = n^t_{x_j}$. The following trivial constraints hold: $\sum_{j=1}^{M} \int d\alpha\, n^t_{x_j,\alpha} = \sum_{j=1}^{M} n^t_{x_j} = \int d\alpha\, n^t_\alpha = N$.

The number of active nodes with activity potential α at time t, denoted with $\mathcal{N}^t_\alpha$, is a random variable given by the sum of M independent binomial distributions (one for each state in $\mathcal{X}$). These distributions are independent because a node can belong to only one state at a given time. Hence,

$$\mathcal{N}^t_\alpha \sim \sum_{j=1}^{M} \mathrm{B}(n^t_{x_j,\alpha}, \eta_{x_j}\alpha), \tag{12}$$

where $\eta_{x_j}\alpha$ is the probability that a node in state x_j with activity potential α becomes active. The expected number of active nodes with a given activity potential α is

$$\mathrm{E}\left[\mathcal{N}^t_\alpha\right] = \sum_{j=1}^{M} \eta_{x_j}\alpha n^t_{x_j,\alpha}. \tag{13}$$

Therefore, the expected number of active nodes can be computed as

$$\begin{aligned}\mathrm{E}\left[\mathcal{N}^t\right] &= \int d\alpha \mathrm{E}\left[\mathcal{N}^t_\alpha\right] = \int d\alpha \sum_{j=1}^{M} \frac{\eta_{x_j}\alpha n^t_{x_j,\alpha} n^t_{x_j}}{n^t_{x_j}} = \\ &= \sum_{j=1}^{M} \eta_{x_j} n^t_{x_j} \int d\alpha \frac{\alpha n^t_{x_j,\alpha}}{n^t_{x_j}} = \sum_{j=1}^{M} \eta_{x_j} \langle \alpha^t_{x_j} \rangle n^t_{x_j},\end{aligned} \tag{14}$$

where $\langle \alpha^t_{x_j} \rangle$ is the average activity potential of nodes in state x_j at time t.

The expected number of links generated in a unit time is $\mathrm{E}\left[L^t\right] = m\mathrm{E}\left[\mathcal{N}^t\right]$. Hence, the expected average degree associated with the time-varying links is

$$\mathrm{E}\left[\langle k^t_{\mathrm{ADN}} \rangle\right] = \frac{2\mathrm{E}\left[L^t\right]}{N} = \frac{2m}{N} \sum_{j=1}^{M} \eta_{x_j} \langle \alpha^t_{x_j} \rangle n^t_{x_j}. \tag{15}$$

If no behavioral change is included, $\eta_{x_j} = \eta\ \forall j$, and the activity rate of a node with activity potential α becomes independent of its state. Then, Eq. (13) reads $\mathrm{E}\left[\mathcal{N}^t_\alpha\right] = n^t_\alpha \eta\alpha$ and Eq. (14) reads $\mathrm{E}\left[\mathcal{N}^t\right] = N\eta\langle\alpha\rangle$. Finally, we recover the claim in [8], that is, $\mathrm{E}\left[\langle k^t_{\mathrm{ADN}} \rangle\right] = 2m\eta\langle\alpha\rangle$. For example, in the SIR model, Eq. (15) specializes to second summand of Eq. (2).

Next, we examine the degree distribution. As discussed in the main paper, our model comprises two independent degree distributions, one for the static backbone and one for the ADN. The former, $P(k_{\mathrm{st}})$, is constant in time and given a priori. The latter varies in time, according to the ADN paradigm. We analytically demonstrate that the time integral of an ADN over a prescribed window yields a degree distribution that shares similarities with the distribution of the activity potential.

We define $\cup_{t=0}^{T} G^t_{\mathrm{ADN}}$ as the union of T consecutive realizations of the ADN. After T aggregations of the ADN, the expected degree of node i, with respect to time-varying links, can be written as $\mathrm{E}[k^T_{\mathrm{ADN},i}] = \mathrm{E}[k^T_{\mathrm{ADN,out},i}] + \mathrm{E}[k^T_{\mathrm{ADN,in},i}]$. The expected out-degree $\mathrm{E}[k^T_{\mathrm{ADN,out},i}]$ corresponds to links generated by i when active, while the in-degree $\mathrm{E}[k^T_{\mathrm{ADN,in},i}]$ corresponds to contacts made by other active nodes. We define $T_{x_j,i}$ as the time spent by node i in the state x_j in the time window T. The following trivial closure relationship must hold: $T = T_i = \sum_{j=1}^{M} T_{x_j,i}$, since all nodes in the ADN share a common integration time.

Node i with activity potential α_i will be active, on average, a number of times equal to the expected values of M binomial distributions, one for each state. Therefore, the expected number of links generated by node i in a time interval T is

$$\begin{aligned}\mathrm{E}[L^T_i] &= \sum_{t=1}^{T} \mathrm{E}[L^t_i] = m \sum_{t=1}^{T} \mathrm{E}\left[\mathcal{N}^t_{\alpha_i}\right] = \\ &= m \sum_{t=1}^{T} \sum_{j=1}^{M} \eta_{x_j}\alpha_i n^t_{x_j,\alpha_i} = m\alpha_i \sum_{j=1}^{M} \eta_{x_j} T_{x_j,i},\end{aligned} \tag{16}$$

where we have used $n^t_{x_j,\alpha_i} = 1$, since we are studying the single node i. Mirroring the analogy with a Polya urn, drawn from [8], we obtain the following expression for the average out-degree:

$$\mathrm{E}[k^T_{\mathrm{ADN,out},i}] \simeq N\left(1 - e^{-\mathrm{E}[L^T_i]/N}\right), \tag{17}$$

in the thermodynamic limit $N \to +\infty$ and for finite T. With respect to the in-degree of node i, we compute the average number of nodes that has been active in the time interval T and multiply this value by the probability that the node has not been contacted by node i in T. In the thermodynamic limit and for finite T, the expected in-degree is

$$\begin{aligned}\mathrm{E}[k^T_{\mathrm{ADN,in},i}] &= \mathrm{E}[L^T]\left(1 - \frac{1}{N}\right)^{-\mathrm{E}[L^T]} \simeq \\ &\simeq \mathrm{E}[L^T] e^{-\mathrm{E}[L^T]/N},\end{aligned} \tag{18}$$

where $\mathrm{E}[L^T]$ is the expected number of edges in the integrated network.

Ultimately, we can combine the expressions for the in- and out-degree in Eqs. (17) and (18) to establish

$$\begin{aligned}\mathrm{E}[k^T_{\mathrm{ADN},i}] &\simeq N\left(1 - e^{-\mathrm{E}[L^T_i]/N}\right) + \mathrm{E}[L^T] e^{-\mathrm{E}[L^T_i]/N} \simeq \\ &\simeq N\left(1 - e^{-\mathrm{E}[L^T_i]/N}\right) \simeq E[k^T_{\mathrm{ADN,out},i}],\end{aligned} \tag{19}$$

which indicates that the expected degree is dominated by the out-degree. By considering Eq. (16), we can write the

activity potential α_i as a function of the expected integrated degree associated with time-varying links, that is,

$$\alpha_i = -\frac{N}{m\sum_{j=1}^{M}\eta_{x_j,i}T_{x_j}}\ln\left(1-\frac{\mathrm{E}[k^T_{\mathrm{ADN},i}]}{N}\right)\simeq \simeq \frac{\mathrm{E}[k^T_{\mathrm{ADN},i}]}{m\sum_{j=1}^{M}\eta_{x_j}T_{x_j,i}}. \tag{20}$$

This relationship supports our claim in Eq. (3), regarding the equivalence of the degree distribution of the integrated network and the distribution of the activity potential. With respect to Eq. (3), ξ corresponds to the right hand side in the last approximation of Eq. (20), yielding Eq. (4) upon specializing to the SIS model.

Analytical computation of the epidemic thresholds

First, we examine an ER network [40], with Poissonian degree distribution $P(k_{\mathrm{s}})$, similarly to [20]. Then, we study an RR network [49], which is expected to offer an improved representation of large random backbones [43], [44], [45].

For an SIR model, Eq. (5) gives the number of infected individuals in the network G^t with activity potential α at time $t+\Delta t$. At the onset of the process, $I^t \sim 1/N$ and $R^t \sim 0$. Summing over all the potentials, neglecting second-order terms in I^t and the terms in R^tI^t, we obtain

$$I^{t+\Delta t} = I^t - \mu\Delta t I^t + \lambda m\eta_S\langle\alpha\rangle\Delta t I^t + \lambda m\eta_I\Delta t\theta^t + \lambda\Delta t\langle k_{\mathrm{st}}\rangle I^t, \tag{21}$$

where $I^t = \int d\alpha I^t_\alpha$ and $\theta^t = \int d\alpha I^t_\alpha\alpha$. Eq. (21) is valid for both SIS and SIR models, whereby an equivalent derivation for the SIS process might be performed to attain the same result. An auxiliary equation can be easily obtained by multiplying all the terms in Eq. (21) by α and integrating over all the activity potentials, namely,

$$\theta^{t+\Delta t} = \theta^t - \mu\Delta t\theta^t + \lambda m\eta_S\langle\alpha^2\rangle\Delta t I^t + \lambda m\eta_I\langle\alpha\rangle\Delta t\theta^t + \lambda\Delta t\langle k_{\mathrm{st}}\rangle\langle\alpha\rangle I^t. \tag{22}$$

Taking the limit as $\Delta t \to 0$ in Eqs. (21) and (22) and reordering all terms, we can write the two equations in the form of Eq. (6).

For an SIS model, Eq. (10) gives the number of infected individuals with activity potential α at time $t+\Delta t$. Summing over all the classes and neglecting second-order terms in I^t, we determine

$$I^{t+\Delta t} = I^t - \mu\Delta t I^t + \lambda m\eta_S\langle\alpha\rangle\Delta t I^t + \lambda m\eta_I\Delta t\theta^t + \lambda\Delta t k_{\mathrm{st}} I^t - \lambda\Delta t k_{\mathrm{st}} U^t. \tag{23}$$

Similar to Eq. (24), an auxiliary equation is obtained by multiplying all terms in Eq. (23) by α and integrating over all the classes, such that,

$$\theta^{t+\Delta t} = \theta^t - \mu\Delta t\theta^t + \lambda m\eta_S\langle\alpha^2\rangle\Delta t I^t + \lambda m\eta_I\langle\alpha\rangle\Delta t\theta^t + \lambda\Delta t k_{\mathrm{st}}\langle\alpha\rangle I^t - \lambda\Delta t k_{\mathrm{st}}\langle\alpha\rangle U^t. \tag{24}$$

The number or pairs in the ADN is neglected in our treatment, since the ADN paradigm inherently leads to a random uncorrelated network. Thus, we should only consider pairs in the backbone. Toward this aim, we multiply the differential equation in the Appendix of [44] by N, to replace the dependence on probability with the number of pairs. Ultimately, we determine

$$\partial_t U = \lambda k_{\mathrm{st}} I + [-\mu k_{\mathrm{st}} - \lambda k_{\mathrm{st}}]\, U, \tag{25}$$

which together with the limit as $\Delta t \to 0$ of Eqs. (23) and (24), yields Eq. (11).

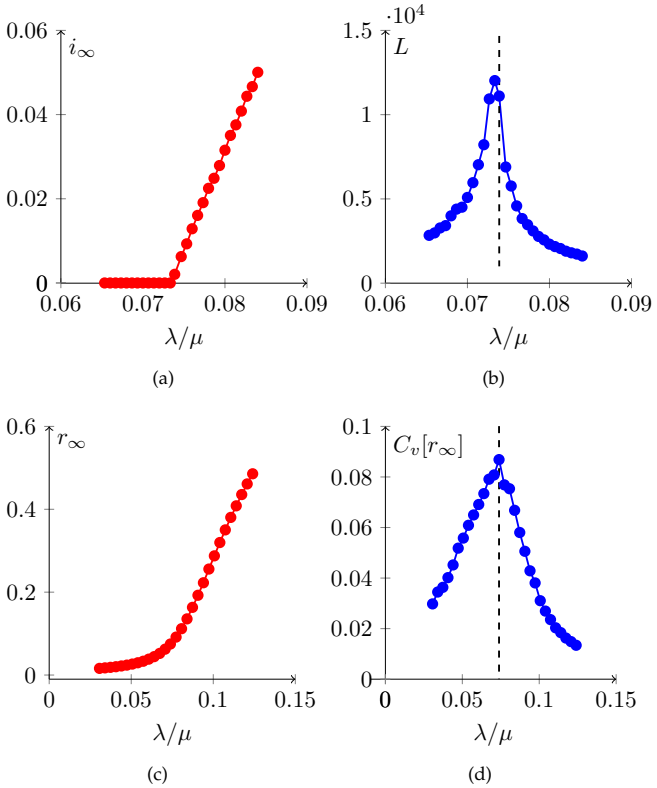

Fig. 7. An exemplary realization of the proposed network model to illustrate our approach to estimate epidemic thresholds. Panel (a): the fraction of infected nodes in the steady state i_∞ as a function of λ/μ. Panel (b): lifetime L as a function of λ/μ. Panel (c): fraction of recovered nodes at the end of the simulation, r_∞, as a function of λ/μ. Panel (d): variance of r_∞ as a function of λ/μ. In all plots, the epidemic threshold, σ, is indicated with a black vertical line. Parameter values are: $N = 10^5$, $T = 10^5$, $\epsilon = 10^{-3}$, $\gamma = 2.1$, $\eta_I = 3$, $\eta_S = 15$, $m = 364$, $\mu = 0.015$, $\langle k_{\mathrm{st}}\rangle = 10$ (ER network), and $C = 0.5$. Median of 10^2 independent simulations. The fraction of random initial infected individuals is set to $0.01N$.

Evaluation of SIS and SIR numerical epidemic thresholds

Here, we present two numerical methods to estimate the SIS and SIR thresholds. The epidemic threshold is a critical value that separates two different regimes: a regime in which the disease eventually dies out and reaches only a local set of nodes in the system and another one where the disease becomes an epidemic and affects a macroscopic fraction of the system.

Our approach to estimate the SIS epidemic threshold is based on [63] and we use Fig. 7 as an illustrative example. In Fig. 7a, we depict the final fraction of nodes in the infected state, i_∞, as a function of the ratio between the infection rate and spontaneous recovery rate, λ/μ. The numerical estimation of i_∞ is challenging, as it requires the determination of the number of infected nodes in the endemic state,

which may hinder the accuracy of the estimation. In Fig. 7b, we show the epidemic threshold, σ, drawn as a vertical dashed black line. It is evaluated by plotting the lifetime L of the simulation as a function of λ/μ. To select a suitable value of L, two other parameters are involved: the number of infected nodes at time t, I^t, and the fraction of nodes infected at least once until time t, called coverage C^t. The lifetime L is evaluated when either one of the following two conditions occurs: i) $I^t = 0$, that is, the disease is no more present in the network; or ii) $C^t = C$, for a fixed value $0 \leq C \leq 1$, that is, the disease has reached a macroscopic fraction and, in the thermodynamic limit, it has a very high probability to infect the whole network. For finite values of N, in [63], it is suggested that the threshold is robust for $C \geq 0.5$; therefore, we set $C = 0.5$ to reduce the computational time. As suggested in [63], the peak in the lifetime L, shown in Fig. 7b, indicates a phase transitions between the disease free regime and the endemic regime. Therefore, the epidemic threshold can be evaluated as the value of λ/μ at which this peak is attained, marked here as a dashed black vertical line.

The epidemic threshold in an SIR model is determined monitoring the fraction of nodes in the recovered state, r_∞, often termed as the epidemic size. In an SIR model, the evaluation of r_∞ does not pose technical challenges, since each realization of the dynamics is finite. In Fig. 7c, we illustrate r_∞ as a function of λ/μ, from which we confirm the intuition that the fraction of nodes in the recovered state grows with λ/μ. However, oscillations around the median are not equally distributed, and the location of the peak of the coefficient of variation might be used to infer the epidemic threshold [50], [51]. More specifically, we maximize the following quantity:

$$C_v[r_\infty] = \frac{\sqrt{\langle r_\infty^2 \rangle - \langle r_\infty \rangle^2}}{r_\infty} \tag{26}$$

For completeness, in Fig. 7d, we display such a coefficient of variation, from which it is possible to predict the epidemic threshold in an SIR model.

In principle, the above mentioned methods do not allow for the construction of confidence intervals around the epidemic thresholds for SIS and SIR models. To offer a statistical framework to systematically evaluate the precision and accuracy of the epidemic threshold we adopt the following approach. First, we discretize the range of λ/μ with a given resolution, chosen on the basis of pilot experiments, as those sketched in Fig. 7. For each value of λ/μ, we run a number of independent simulations (10^2 for the SIS and 10^3 SIR model). As sketched in Fig. 7, we obtain a set of independent estimates of the epidemic thresholds (10^2 for the SIS and 10^3 SIR model) by monitoring the lifetime L for the SIS model and the coefficient of variation C_v for the SIR model. We resample with replacement this set a large number of times (10^2 for the SIS and 10^3 SIR model) and compute the median of each resampled dataset. From these, we estimate a global median, which corresponds to our inference of the epidemic threshold, and 95% confidence intervals, which represent our error bars. Should the confidence interval be less than the initial resolution for λ/μ, we would use the initial resolution.

(a)

SIS	Network	$\eta_I/\eta_S = 0$	$\eta_I/\eta_S = 0.2$
Theory ($N \to +\infty$)	$k_{\rm st} = 0$	**0.250**	0.094
	ER	0.167	**0.121**
	RR	0.186	**0.127**
Numerics ($N = 2 \cdot 10^5$)	$k_{\rm st} = 0$	**0.260 (0.250, 0.273)**	0.100 (0.097, 0.103)
	ER	0.167 (0.160, 0.173)	**0.121 (0.117, 0.123)**
	RR	0.186 (0.180, 0.193)	**0.127 (0.123, 0.130)**
Numerics ($N = 1 \cdot 10^5$)	$k_{\rm st} = 0$	**0.260 (0.250, 0.273)**	0.100 (0.097, 0.103)
	ER	0.167 (0.160, 0.173)	**0.123 (0.121, 0.125)**
	RR	0.186 (0.180, 0.193)	**0.127 (0.123, 0.130)**
Numerics ($N = 0.5 \cdot 10^5$)	$k_{\rm st} = 0$	**0.273 (0.260, 0.287)**	0.097 (0.094, 0.100)
	ER	0.167 (0.160, 0.173)	**0.123 (0.121, 0.127)**
	RR	0.186 (0.180, 0.193)	**0.130 (0.127, 0.133)**
Numerics ($N = 0.2 \cdot 10^5$)	$k_{\rm st} = 0$	**0.260 (0.250, 0.273)**	0.097 (0.094, 0.100)
	ER	0.167 (0.160, 0.173)	**0.123 (0.121, 0.127)**
	RR	0.193 (0.186, 0.200)	**0.133 (0.130, 0.137)**

(b)

SIR	Network	$\eta_I/\eta_S = 0$	$\eta_I/\eta_S = 0.2$
Theory ($N \to +\infty$)	$k_{\rm st} = 0$	**0.250**	0.094
	ER	0.167	**0.121**
	RR	0.186	**0.127**
Numerics ($N = 2 \cdot 10^5$)	$k_{\rm st} = 0$	**0.273 (0.260, 0.294)**	0.087 (0.083, 0.090)
	ER	0.173 (0.167, 0.180)	**0.113 (0.110, 0.121)**
	RR	0.193 (0.186, 0.200)	**0.123 (0.120, 0.127)**
Numerics ($N = 1 \cdot 10^5$)	$k_{\rm st} = 0$	**0.260 (0.250, 0.273)**	0.087 (0.083, 0.090)
	ER	0.171 (0.168, 0.173)	**0.115 (0.112, 0.117)**
	RR	0.200 (0.193, 0.207)	**0.123 (0.120, 0.127)**
Numerics ($N = 0.5 \cdot 10^5$)	$k_{\rm st} = 0$	**0.273 (0.260, 0.287)**	0.100 (0.097, 0.103)
	ER	0.180 (0.173, 0.187)	**0.113 (0.110, 0.121)**
	RR	0.186 (0.180, 0.193)	**0.127 (0.123, 0.130)**
Numerics ($N = 0.2 \cdot 10^5$)	$k_{\rm st} = 0$	**0.273 (0.260, 0.287)**	0.094 (0.083, 0.097)
	ER	0.173 (0.167, 0.180)	**0.113 (0.110, 0.121)**
	RR	0.180 (0.173, 0.193)	**0.123 (0.120, 0.127)**

TABLE 1
Epidemic thresholds as functions of η_I/η_S for various network sizes. Theoretical predictions refer to the thermodynamic limit, $N \to +\infty$, and obtained from Eqs. (7) and (9) for the SIS model and through stability analysis of Eq. (11) for the SIR model. Numerical results are displayed alongside with the network size. For each pair (N, η_I/η_S), we compare the thresholds with and without backbone, highlighting the highest values in bold. For ER and RR backbones, we choose $\langle k_{\rm st} \rangle = 4$ and $m = 364$; for pure ADN, $\langle k_{\rm st} \rangle = 0$ and m = 728. We set $\eta_S = 15$ and $\eta_I \in \{0, 3\}$. Other parameter values are: $T = 10^5$, $\epsilon = 10^{-3}$, $\gamma = 2.1$, and $\mu = 0.015$. For the numerical computations, data are reported as medians of 10^2 independent simulations for the SIS model, and 10^3 for the SIR model. The fraction of random initial infected individuals is set to $0.01N$. Values in parentheses indicate 95% confidence intervals.

Analysis of network size

Here, we present numerical evidence to exclude the possibility that the cross over between the epidemic thresholds with and without the static backbone, demonstrated in Fig. 3, is a numerical artifact of the finite size of the network. More specifically, we report simulation results for several network sizes, $N = 2{\cdot}10^5$, $N = 1{\cdot}10^5$, $N = 0.5{\cdot}10^5$, and $N = 0.2{\cdot}10^5$, using the same parameter set of Fig. 3. Simulation results are presented in Table 1, along with theoretical predictions in the thermodynamic limit. In agreement with theoretical predictions in the thermodynamic limit, for both SIS and SIR models, for any choice of the network size we confirm that in the absence of behavioral changes, the largest value of the threshold is attained without the static backbone. On the other hand, for $\eta_I/\eta_S = 0.2$, the epidemic threshold is higher in the presence of a static backbone, let it be an ER or a RR network.